quence against each consensus sequence revealed no similarity. Additional comparisons with the sequences of mouse, rat, canine, or human TPO were performed with the MacDNASIS Pro (Hitachi) homology match program (based on the Lipman-Pearson algorithm). No similarity was detected with a cutoff score >20 (Ktup value, the minimum number of consecutive residues that must match in a homology region in order for a score to be assigned, was set to 2).
15. C. M. Gates, W. P. Stemmer, R. Kaptein, P. J. Schatz, *J. Mol. Biol.* **255**, 373 (1996).
16. We constructed mutagenesis library ON3396 by cloning oligonucleotides containing the sequence $(NNK)_5$ YST acK ctK cgK NaK tNK NtK $(NNK)_7$ into the headpiece dimer vector. We constructed library ON3410 by cloning oligonucleotides containing the sequence $(NNK)_4$ YST acK ctK cgK NaK tNK NtK $(NNK)_6$ TST into the polysome display system. Nucleotide abbreviations: Y = C or T; S = G or C; N = A, C, G, or T; K = G or T. Lowercase letters represent a mixture of 70% of the indicated base and 10% of each of the other three nucleotides. The degenerate codon YST encodes Cys, Ser, Pro, and Arg.
17. L. C. Mattheakis, R. R. Bhatt, W. J. Dower, *Proc. Natl. Acad. Sci. U.S.A.* **91**, 9022 (1994); L. C. Mattheakis, J. M. Dias, W. J. Dower, *Methods Enzymol.* **267**, 195 (1996).
18. Rounds 1 and 2 were performed with standard procedures (*13*, *15*). In rounds 3 and 4, 100 μM AF12191 was added to wells containing the receptor-bound plasmid complexes and incubated at 4°C for 45 min to accelerate the dissociation of lower-affinity peptides.
19. Automated "split and pool" oligonucleotide synthesis (*26*) generated a collection of oligonucleotides that encode the peptide sequence LAIEGPTLRQWLHGNGRDT in which the underlined amino acids were held constant and the remaining positions were either deleted, substituted with alanine, or conserved.
20. R. Palacios and M. Steinmetz, *Cell* **41**, 727 (1985).
21. Full-length huTPOR cDNA (628–amino acid P-form) (*2*) was isolated from KG-1 cell mRNA with primers that allowed insertion into the Xho I and EcoR I sites of the α+ vector. Expression of the receptor is under the control of the SRα promoter. Fifty micrograms of the α+ TPOR vector was electroporated into ~10^7 Ba/F3 cells. Selection was done in cell media (RPMI 1640, 10% fetal calf serum, 2 mM l-glutamine, 1× antibiotics–antimycotics) supplemented with WEHI-3 conditioned medium (10%) and G418 (1 mg/ml). G418-resistant cells were clone-sorted, and TPO-responsive clones were selected in media (RPMI 1640, 15% fetal calf serum, 2 mM l-glutamine, 1× antibiotics–antimycotics) supplemented with 1% supernatant from COS-7 cells transiently expressing full-length rhTPO.
22. D. J. Duffin *et al.*, unpublished data.
23. N. C. Wrighton *et al.*, *Blood* **88** (suppl. 1), 543a (1996).
24. The first synthesis cycle coupled 9-fluorenyl methoxycarbonyl (FMOC)–lysine (Allyloxycarbonyl protected ε-amino group) to the PAL resin (Millipore). The FMOC-protecting group was removed, followed by coupling with FMOC–β-Ala. The third cycle began with the removal of the Alloc protecting group with $[(C_6H_5)_3P]_4Pd$–4-methylmorpholine–chloroform, followed by removal of the α-amino FMOC-group. Synthesis on both branches proceeded with standard FMOC-coupling chemistry.
25. H. M. McConnell *et al.*, *Science* **257**, 1906 (1992).
26. E. A. Peters, P. J. Schatz, S. J. Johnson, W. J. Dower, *J. Bacteriol.* **176**, 4296 (1994).
27. Peptides were prepared by automated solid-phase synthesis and purified by C18 reversed-phase high-performance liquid chromatography (HPLC). Intramolecular oxidation of the thiols in cysteine-containing peptides was achieved by overnight incubation in 20% dimethyl sulfoxide (DMSO)–water, followed by purification of the cyclized peptide by reversed-phase HPLC. The structures of the purified peptides were confirmed by electrospray mass spectrometry.
28. S. Ymer *et al.*, *Nature* **317**, 255 (1985).
29. Human bone marrow aspirated from the posterior iliac crest was collected in preservative-free heparin from normal, volunteer donors with informed consent. Bone marrow mononuclear cells were isolated by density centrifugation with Ficoll-Paque 1077, washed three times with Hepes-buffered saline, and resuspended in RPMI 1640 containing 5% human platelet-depleted plasma [R. Dornsife *et al.*, *Antimicrob. Agents Chemother.* **35**, 322 (1991)]. The preparation was enriched for $CD34^+$ cells with a StemSep lineage depletion kit (StemCell Technologies, Vancouver, BC).
30. We thank E. Tate, T. Dias, Y. Feng, E. Whitehorn, and M. Bremer (receptor cloning and expression); R. Raab, G. Dawes, and C. Iverson (oligonucleotide synthesis and DNA sequencing); S. Podduturi and Q. Yin (peptide synthesis); S. Piplani, S. Johnson, and J. Dias (library screening); T. Cutler (proliferation assays) of the Affymax Research Institute; and A. Lee, I. Dev (human bone marrow assays), S. Rudolph, C. Merrell, and J. Dillberger (in vivo efficacy studies) of the Glaxo Wellcome Research Institute.

20 February 1997; accepted 21 April 1997

Epilepsy and Exacerbation of Brain Injury in Mice Lacking the Glutamate Transporter GLT-1

Kohichi Tanaka,* Kei Watase, Toshiya Manabe, Keiko Yamada, Masahiko Watanabe, Katsunobu Takahashi, Hisayuki Iwama, Toru Nishikawa, Nobutsune Ichihara, Tateki Kikuchi, Shigeru Okuyama, Naoya Kawashima, Seiji Hori, Misato Takimoto, Keiji Wada

Extracellular levels of the excitatory neurotransmitter glutamate in the nervous system are maintained by transporters that actively remove glutamate from the extracellular space. Homozygous mice deficient in GLT-1, a widely distributed astrocytic glutamate transporter, show lethal spontaneous seizures and increased susceptibility to acute cortical injury. These effects can be attributed to elevated levels of residual glutamate in the brains of these mice.

The extracellular concentration of the excitatory neurotransmitter L-glutamate in the mammalian central nervous system must be kept low to ensure a high signal-to-noise ratio during synaptic activation and to prevent neuronal damage from excessive activation of glutamate receptors (*1*). This control is achieved by high-affinity, Na^+-dependent glutamate transporters in the plasma membrane of neurons and surrounding glial cells (*2*). The failure or reversal of these transporters may contribute to cellular damage in stroke, trauma, Alzheimer's disease, amyotrophic lateral sclerosis, and Huntington's disease (*3*). Four subtypes of glutamate transporters have been defined by differences in sequence, pharmacology, tissue distribution, and channel-like properties: GLAST, GLT-1, EAAC1, and EAAT4 (*4*). EAAC1 and EAAT4 are selectively localized to neurons, whereas GLT-1 and GLAST are astroglial transporters (*5*). However, the roles of glutamate transporter subtypes in synaptic transmission and neurotoxicity are not known because subtype-specific inhibitors are not available. We therefore generated mice that lack GLT-1, using homologous recombination.

To disrupt the mouse gene encoding GLT-1 in E14 embryonic stem (ES) cells by homologous recombination, we constructed a targeting vector in which the exon encoding the putative third transmembrane segment was replaced with the neomycin resistance gene (Fig. 1A). Four targeted clones were identified from 144 G418- and gancyclovir (GANC)–resistant clones by Southern (DNA) blotting with 5′-flanking and 3′-flanking probes (Fig. 1A). Two mutant clones were separately injected into C57BL/6J blastocysts to produce chimeric animals. Heterozygous animals were identified by Southern blotting and were bred with each other to obtain homozygous animals, which showed the proper structure of the GLT-1 gene by Southern analysis (Fig. 1B). Northern (RNA) blotting showed that brains from homozygous mutant mice contain a hybridizable transcript that is similar in size to the wild-type GLT-1 mRNA (Fig. 1C). Reverse transcription–polymerase chain reaction experiments, followed by Southern blot analysis with an exon-specif-

K. Tanaka, K. Watase, K. Wada, Department of Degenerative Neurological Diseases, National Institute of Neuroscience, Kodaira, Tokyo 187, Japan.
T. Manabe, Department of Neurophysiology, Faculty of Medicine, University of Tokyo, Tokyo 113 Japan.
K. Yamada and M. Watanabe, Department of Anatomy, Hokkaido University School of Medicine, Sapporo 060, Japan.
K. Takahashi, H. Iwama, T. Nishikawa, Department of Mental Disorder Research, National Institute of Neuroscience, Kodaira, Tokyo 187, Japan.
N. Ichihara and T. Kikuchi, Department of Animal Models for Human Disease, National Institute of Neuroscience, Kodaira, Tokyo 187, Japan.
S. Okuyama and N. Kawashima, 1st Laboratory, Medicinal Research Laboratories, Taisho Pharmaceutical Co., 1-403 Yoshino-cho, Ohmiya-shi, Saitama 330, Japan.
S. Hori and M. Takimoto, International Research Laboratories, Ciba-Geigy Japan, 10-66, Miyuki-cho, Takarazuka 665, Japan.

*To whom correspondence should be addressed. E-mail: tanaka@ncnaxp.ncap.go.jp

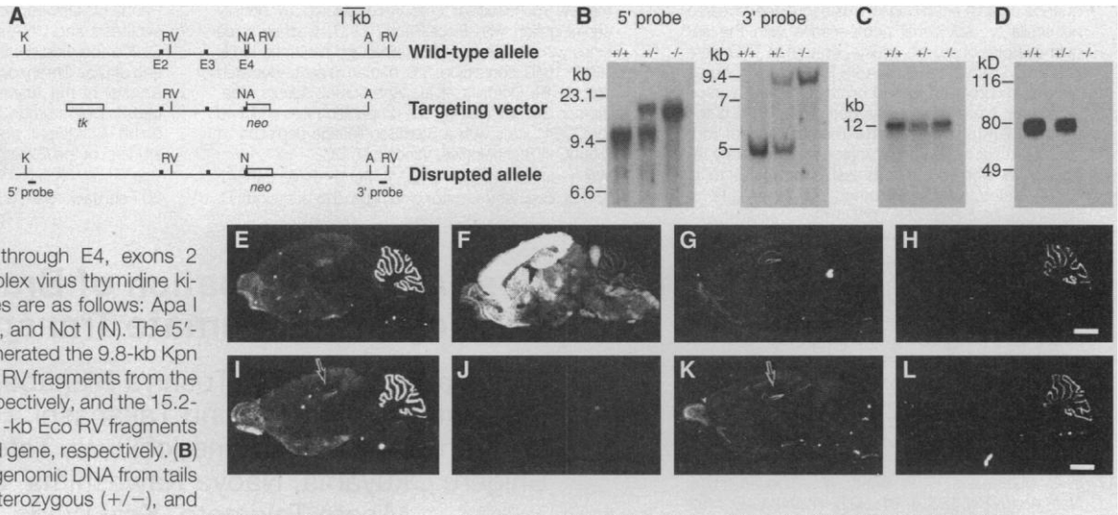

Fig. 1. Targeted disruption of the mouse gene encoding GLT-1. (**A**) Homologous recombination resulted in replacement of the 0.8-kb fragment from the GLT-1 gene, including 224 bp of exon 4 with the neomycin resistance gene (*neo*). Closed boxes E2 through E4, exons 2 through 4; *tk*, herpes simplex virus thymidine kinase gene. Restriction sites are as follows: Apa I (A), Eco RV (RV), Kpn I (K), and Not I (N). The 5′- and 3′-flanking probes generated the 9.8-kb Kpn I–Apa I and the 5.0-kb Eco RV fragments from the wild-type GLT-1 gene, respectively, and the 15.2-kb Kpn I–Apa I and the 9.1-kb Eco RV fragments from the properly disrupted gene, respectively. (**B**) Southern blot analyses of genomic DNA from tails of the wild-type (+/+), heterozygous (+/−), and homozygous mutant mice (−/−). Kpn I–Apa I–digested DNAs and Eco RV–digested DNAs were hybridized with the 5′-flanking probe (left) and 3′-flanking probe (right), respectively. (**C**) Northern blot analysis of cerebral RNAs from the wild-type (+/+), heterozygous (+/−), and homozygous mutant (−/−) mice. (**D**) Protein immunoblot analysis of cerebral membrane fractions with antibody to GLT-1. (**E** through **L**) In situ hybridization analysis of the parasagittal brain sections of the wild-type [(E) through (H)] and mutant [(I) through (L)] mice at the second postnatal month with oligonucleotide probes specific for the GLAST [(E) and (I)], GLT-1 [(F) and (J)], EAAC1 [(G) and (K)], and EAAT4 [(H) and (L)] mRNAs. Arrows indicate the hippocampal CA1 region in the mutant, which lacks the GLAST and EAAC1 mRNAs. Scale bars, 2 mm.

ic probe corresponding to the disrupted region, indicated that the transcript derived from the mutated allele lacks exon 4 (6). However, protein immunoblot analysis (Fig. 1D) detected no GLT-1 protein in the brains of the mutant mice (7). By in situ hybridization with oligonucleotide probes, expression of the four glutamate transporter subtypes was examined in the brains of wild-type and mutant mice (Fig. 1, E to L) (8). Hybridization signals for GLT-1 disappeared completely from the mutant brain (Fig. 1J). The levels of the other glutamate transporter subtype mRNAs were not appreciably affected by mutation. Glutamate uptake in cortical crude synaptosomes of mutant mice was decreased to 5.8% of that in synaptosomes from wild-type mice [mean ± SEM (three animals per group) for the Michaelis constant (K_m) (at micromolar concentration) and the maximum uptake velocity (V_{max}) (in picomoles per minute per milligram of protein) are, respectively: wild type, 46.1 ± 4.2, 19,716.2 ± 7280.2; mutant, 22.1 ± 0.46, 1139.0 ± 432.1], which suggests that GLT-1 is responsible for the greatest proportion of cerebral glutamate transport (9).

Mice heterozygous for GLT-1 were indistinguishable from wild-type mice. Homozygous mice were born from heterozygous crosses at the frequency predicted by Mendelian ratios (n = 312): 24.4% wild type, 50.6% heterozygous, and 25.0% homozygous. The body weight and general appearance of the homozygous mice were normal at birth, but homozygous mice gained weight more slowly than did wild-type mice (Fig. 2A) and tended to die prematurely (50.0% survival after 6 weeks) (Fig. 2B). Deaths were not preceded by any noticeable health problems. Postmortem analyses revealed no evidence of hemorrhage, infarction, or ischemia that might be associated with cardiovascular failure or stroke and no gross abnormalities in skeletal muscles or visceral organs. However, continuous videotape monitoring of small groups of mice revealed the occurrence of spontaneous epileptic seizures with behavioral patterns similar to those of *N*-methyl-D-aspartate (NMDA)–induced seizures (*10*), characterized by explosive running followed by maintained opisthotonus and straub tail (Fig. 2C). In most cases, these mice died within a few minutes of seizure onset. A subset of mutant mice quickly recovered and resumed apparently normal behavior but developed additional seizures and died later.

To confirm profound hyperexcitability in mutant mice, we compared the electroencephalogram (EEG) patterns of wild-type and homozygous mutant mice treated with the convulsant agent pentylenetetrazole (PTZ), a γ-aminobutyric acid receptor antagonist (*11*). After a single injection of PTZ at a subconvulsive dose of 30 mg per kilogram of body weight (30 mg/kg), high-voltage sharp wave bursts unaccompanied by behavioral changes were detected in mutant mice, whereas no epileptiform discharges were observed in wild-type mice

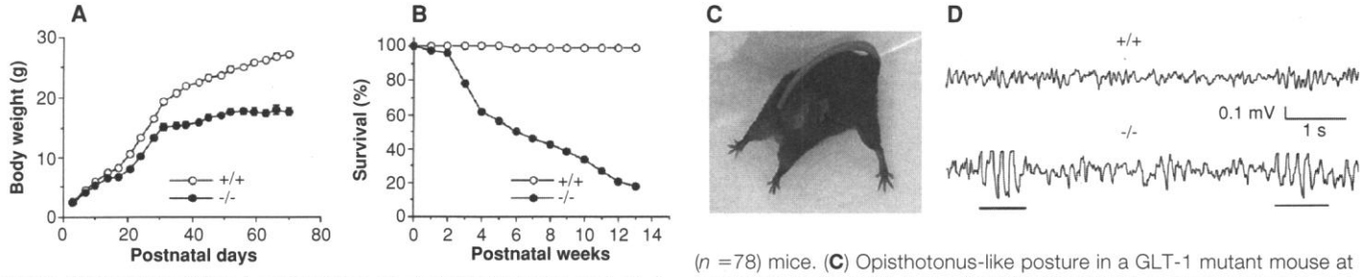

Fig. 2. Phenotypes of GLT-1 mutant mice. (**A**) Body weight (mean ± SEM) of homozygous (−/−) (n = 50) and wild-type (+/+) (n = 58) mice. (**B**) Percentage of postnatal survival of wild-type (+/+) (n = 76) and homozygous (−/−) (n =78) mice. (**C**) Opisthotonus-like posture in a GLT-1 mutant mouse at postnatal day 35 (P35). (**D**) EEG of wild-type (+/+) and homozygous (−/−) mice after PTZ administration. The high-voltage sharp wave bursts are underlined.

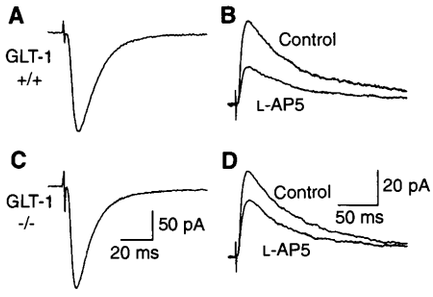

Fig. 3. Kinetics of glutamatergic synaptic responses and estimation of an increase in glutamate concentrations in the synaptic cleft in hippocampal slices of GLT-1 mutant mice. (**A**) The non-NMDA receptor–mediated EPSC in the wild-type mouse recorded from a CA1 pyramidal cell with whole-cell patch-clamp techniques at a holding membrane potential of −90 mV. The time constant of the decaying phase of the current in this cell was 12.4 ms. All the traces were an average of 10 consecutive responses. (**B**) The NMDA receptor–mediated EPSC in the wild-type mouse (control). The decay time constant was 50.1 ms. Application of 400 μM L-AP5, a low-affinity NMDA receptor antagonist, caused a large inhibition of the current (L-AP5). (**C**) The non-NMDA receptor–mediated EPSC in the mutant mouse. The decay time constant was 11.7 ms. (**D**) The NMDA receptor–mediated EPSC in the mutant mouse (control). The decay time constant was 49.2 ms.

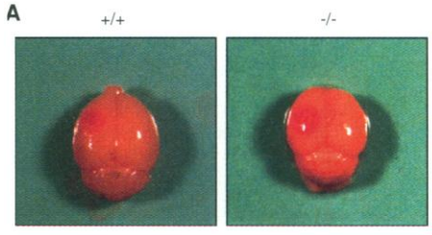

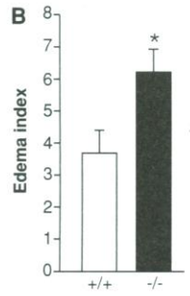

Fig. 5. Wild-type and mutant mouse brains subjected to cold-induced injury to the left cerebral hemisphere. (**A**) Vasogenic edema of wild-type (+/+) and homozygous (−/−) littermates after cold-induced brain injury. (**B**) Comparison of edema formation between wild-type (+/+) (n = 9) and homozygous (−/−) (n = 9) mice after cold-induced injury to the left cerebral hemisphere. Values are mean ± SEM. Asterisk indicates $P < 0.05$ compared to edema index (*20*) of wild-type controls, with the use of the Tukey test.

(Fig. 2D). GLT-1 maps to the central region of mouse chromosome 2 (*12*), near the region of the quantitative trait locus EL-2 of the mouse epilepsy strain (*13*).

To study the role of GLT-1 at central glutamatergic synapses, we performed electrophysiological analysis in the hippocampal CA1 pyramidal neurons (*14*). In CA1 hippocampal pyramidal neurons, stimulation of the afferent fibers led to the generation of an excitatory postsynaptic current (EPSC) that contained both the slow NMDA and fast non-NMDA components. No significant difference in the time course of non-NMDA receptor–mediated EPSCs recorded at −90 mV was found between the wild-type [decay time constant, 11.5 ± 0.8 ms (mean ± SEM); n = 8] and mutant (12.5 ± 0.6 ms; n = 7) slices (Fig. 3, A and C). There was no clear difference in the decay time course of NMDA receptor–mediated EPSCs between the wild-type (55.7 ± 1.9 ms; n = 11) and mutant mice (51.4 ± 2.2 ms; n = 9) (Fig. 3, B and D). These results indicate that GLT-1 does not determine the decay rate of EPSCs in the hippocampus and are consistent with the observation that glutamate transporter blockers have no effect on the decay of EPSCs in the hippocampus (*15*).

We next estimated the peak concentration and time course of free glutamate in the synaptic cleft by analyzing the displacement of a rapidly dissociating NMDA receptor antagonist, L-2-amino-5-phosphonopentanoic acid (L-AP5), from NMDA receptors during synaptic transmission (*16*). The inhibition of NMDA EPSCs by 400 μM L-AP5 in the mutant slices (26.1 ± 4.6%; n = 6) was significantly less than in the wild-type slices (53.0 ± 4.0%; n = 9) ($P < 0.001$), implying that the peak concentration of synaptically released glutamate is increased in mutant mice and that glutamate remains elevated in the synaptic cleft for longer periods in mutant mice (Fig. 3, B and D). These results suggest that GLT-1 is an important determinant of the clearance of free glutamate from the synaptic cleft. A recent study suggests that the uptake rate of GLT-1 is significantly slower than the predicted time course of synaptically released glutamate (*17*). Thus, it is likely that binding to the transporter rather than uptake per se removes glutamate from the cleft. Our observation could be accounted for by the absence of glutamate binding sites.

Because excessive synaptic glutamate leads to neuronal degeneration, we performed systematic histological analysis of the entire brain (*18*). We observed selective neuronal degeneration in the hippocampal CA1 field in 7 of 22 homozygous mutant mice aged 4 to 8 weeks (Fig. 4, A through D). Differences in the selective destruction of hippocampal neurons among individuals likely reflect differences in the occurrence of spontaneous seizures. No obvious morphological abnormalities were found elsewhere (*19*). These results suggest that GLT-1 is essential for maintaining low extracellular glutamate concentrations and for preventing glutamate neurotoxicity. Because GLT-1 is distributed uniformly throughout the hippocampus, another mechanism that is responsible for the selective neuronal vulnerability in the hippocampal CA1 field of mutant mice may exist, a proposal that can be readily investigated in GLT-1 mutant mice.

Experimental induction of injury and ischemia is associated with a large, almost immediate increase in extracellular glutamate concentration (*20*). To examine the role of GLT-1 in the pathogenesis of acute brain injury, we compared edema development after cold-induced injury in wild-type and mutant mice (*21*, *22*). The homozygous mutant mice were significantly more susceptible to edema than were the wild-type mice (Fig. 5A). Edema was 68% greater in the homozygous mutant mice than in the wild-type mice ($P <$ 0.05), and edema size was visibly larger in mutant mice than wild-type mice (Fig. 5B). Our results suggest that GLT-1 normally contributes to the prevention of acute glutamate neurotoxicity after trauma.

Our results indicate that GLT-1 contributes to the maintenance of extracellular glutamate concentrations at low levels. Without its action, glutamate levels rise enough to cause epilepsy and cell death.

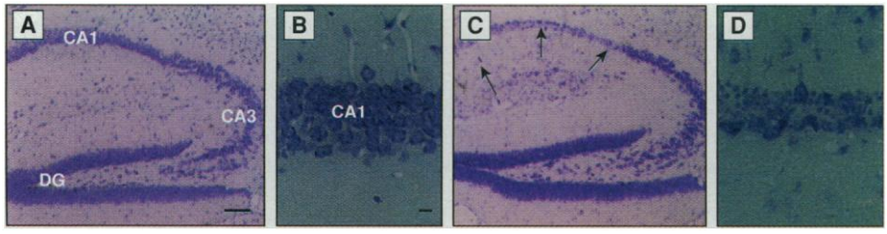

Fig. 4. Selective neuronal degeneration in the hippocampal CA1 of the GLT-1 mutant mouse (**C** and **D**) at P56 as compared to that in the wild-type mouse (**A** and **B**). (A through D) Nissl staining. Selective neuronal loss and residual nuclear debris in the hippocampal CA1 pyramidal layer of the mutant mouse are shown [arrows in (C)]. DG, dentate gyrus. Scale bar in (A), 100 μm; in (B), 10 μm.

REFERENCES AND NOTES

1. D. W. Choi, *Neuron* **1**, 623 (1988).
2. B. I. Kanner and S. Schuldiner, *CRC Crit. Rev. Biochem.* **22**, 1 (1987).
3. M. Szatkowski and D. Attwell, *Trends Neurosci.* **17**, 359 (1994); A. M. Palmer, A. W. Procter, G. C. Stratmann, D. M. Bowen, *Neurosci. Lett.* **66**, 199 (1986); J. D. Rothstein, M. V. Kammen, A. I. Levey, L. J. Martin, R. W. Kuncl, *Ann. Neurol.* **38**, 73 (1995); C. Portera-Cailliau, J. C. Hedreen, D. L. Price, V. E. Koliatsos, *J. Neurosci.* **15**, 3775 (1995).
4. T. Storck, S. Schulte, K. Hofmann, W. Stoffel, *Proc. Natl. Acad. Sci. U.S.A.* **89**, 10,955 (1992); G. Pines *et al.*, *Nature* **360**, 464 (1992); Y. Kanai and M. A. Hediger, *ibid.*, p. 467; K. Tanaka, *Neurosci. Res.* **16**, 149 (1993); W. A. Fairman, R. J. Vandenberg, J. L. Arriza, M. P. Kavanaugh, S. G. Amara, *Nature* **375**, 599 (1995).
5. J. D. Rothstein *et al.*, *Neuron* **13**, 713 (1994); K. Yamada *et al.*, *NeuroReport* **7**, 2013 (1996).
6. K. Tanaka *et al.*, data not shown.
7. The mouse gene encoding GLT-1 was isolated from a mouse genomic library prepared from 129/SvJ mouse DNA (Stratagene) by hybridization with the 763–base pair (bp) Nco I fragment of the mouse GLT-1 cDNA [Y. Mukainaka, K. Tanaka, T. Hagiwara, K. Wada, *Biochim. Biophys. Acta* **1244**, 233 (1995)] used as a probe. The gene comprised 11 exons spanning more than 78 kb [K. Tanaka *et al.*, *Soc. Neurosci. Abstr.* **21**, 1862 (1995)]. The targeting vector consisted of the 11.6-kb genomic sequence in which the 0.8-kb Not I–Eco RV fragment encoding a part of the transmembrane region of GLT-1 was replaced with the 1.2-kb neomycin gene derived from pMC1 neopolyA. A 1.9-kb herpes simplex virus thymidine kinase gene fragment was attached to the 5′ end of the GLT-1-neomycin fragment for negative selection. E14 ES cells were transfected with Kpn I–digested targeting vector by electroporation and selected with G418 and GANC. ES cell lines with targeted disruption of the GLT-1 gene were identified by Southern blot analysis, and targeted clones were obtained with a frequency of 1/36. Injection of ES cells into blastocysts was performed as described [A. P. McMahon and A. Bradley, *Cell* **62**, 1073 (1990)]. RNA blot analysis was carried out by hybridization of total cerebral RNA (10 μg) with the 785-bp Eco RV–Hind III fragment of the mouse GLT-1 cDNA. Crude membrane preparations from mice cerebra were separated by 5 to 15% gradient SDS–polyacrylamide gel electrophoresis, transferred to nitrocellulose, and analyzed by the ECL detection system (Amersham). The antibody to GLT-1 was raised against the COOH-terminal part of GLT-1 (from Leu^{500} to Lys^{525}).
8. In situ hybridization analysis was performed on the parasagittal brain sections as described [T. Shibata, M. Watanabe, K. Tanaka, K. Wada, Y. Inoue, *NeuroReport* **7**, 705 (1996)]. Antisense oligonucleotide probes were as follows: for GLAST, CACATTATCACCGCGACCAATCGCATGATGGCTTCGTTAAGAGAA; for GLT-1, TCGTCGTTCTTCTTCCCGGGCCCTAGCTGCTTCTTGAGTTTGGGA; for EAAC1, ATCGCCCACAGGCTTCACCTCTTCCCGCTTGGTTTTGTACTGCTGA; and for EAAT4, GCCCCCAGCTCTGAACCATTGTCTGTCCTTACAATTGTCCTTGTCA.
9. Crude synaptosomes were prepared from the cortex, and glutamate transport was measured as described [M. B. Robinson, M. Hunter-Ensor, J. Sinor, *Brain Res.* **544**, 196 (1991)]. The synaptosomal preparation (15 to 30 μg of protein per tube) was incubated with 5×10^5 decay per minute of L-[^{3}H]glutamate (54.1 Ci/mmol; New England Nuclear) and with increasing concentrations of glutamate (0 to 300 μM) for 3 min at 37°C in a final volume of 250 μl. Sodium-dependent uptake was calculated to be the difference between the amount of radioactivity obtained in the presence of Na^+ and the amount obtained in the choline-containing buffer. Experiments were done in triplicate for each concentration. The data were analyzed with a nonlinear least-squares curve-fitting technique.
10. M. A. Rogawski *et al.*, *J. Pharmacol. Exp. Ther.* **249**, 708 (1989).
11. To record EEGs, stainless steel flat electrodes were placed on the parietal and frontal portions of the dura mater. In GLT-1 mutant mice, the EEG recordings were normal in the absence of PTZ.
12. M. A. Kirschner, N. G. Copeland, D. J. Gilbert, N. A. Jenkins, S. G. Amara, *Genomics* **24**, 218 (1994).
13. M. L. Rise, W. N. Frankel, J. M. Coffin, T. N. Seyfried, *Science* **253**, 669 (1991).
14. Wild-type or mutant mice 5 to 7 weeks old were decapitated under halothane anesthesia, and hippocampi were quickly removed. Recordings were made from hippocampal slices (400 μm thick) at 26° to 28°C [T. Manabe, D. J. A. Wyllie, D. J. Perkel, R. A. Nicoll, *J. Neurophysiol.* **70**, 1451 (1993)]. To evoke synaptic responses, stimuli (0.1 Hz) were delivered through fine bipolar tungsten electrodes placed in the stratum radiatum. The non-NMDA component could be isolated by holding the cell at potentials more negative than −80 mV. NMDA receptor–mediated EPSCs were recorded with 6-cyano-7-nitroquinoxaline-2,3-dione (CNQX) (20 μM) present to block non-NMDA receptor–mediated EPSCs, and the membrane potential was clamped at +40 mV to remove the voltage-dependent Mg^{2+} block of the NMDA receptor. The values of the membrane potential were corrected for the liquid-junction potential at the electrode tip (−10 mV). Series and input resistances were monitored throughout the experiment. The time constant of the decaying phase of synaptic currents was calculated by fitting a single exponential curve. CNQX and L-AP5 were obtained from Tocris Cookson (Bristol, U.K.).
15. J. S. Isaacson and R. A. Nicoll, *J. Neurophysiol.* **70**, 2187 (1993).
16. J. D. Clements, R. A. Lester, G. Tong, C. E. Jahr, G. L. Westbrook, *Science* **258**, 1498 (1992).
17. J. I. Wadiche, J. L. Arriza, S. G. Amara, M. P. Kavanaugh, *Neuron* **14**, 1019 (1995).
18. The wild-type and GLT-1 mutant mice were fixed transcardially with 4% paraformaldehyde in 0.1 M sodium phosphate buffer and embedded in paraffin wax. Five-micrometer paraffin sections were stained with toluidine blue for Nissl staining.
19. K. Tanaka *et al.*, data not shown.
20. A. I. Faden, P. Demediuk, S. S. Painter, R. Vink, *Science* **244**, 798 (1989); T. K. McIntosh, R. Vink, H. Soares, R. Hayes, R. Simon, *J. Neurochem.* **55**, 1170 (1990).
21. T. D. Oury, C. A. Piantadois, J. D. Crapo, *J. Biol. Chem.* **268**, 15394 (1993).
22. Mice were anesthetized by intraperitoneal injection of pentobarbital (60 mg/kg). An incision was then made in the scalp, and a metal probe 3 mm in diameter, cooled in liquid nitrogen, was placed on the skull over the left cerebral hemisphere for 10 s. The skin incision was then sutured. After the injury (110 min) the mouse was perfused transcardially with 20 ml of saline. The right (R) and left (L) cerebral hemispheres were separated and immediately weighed (wet weight, *W*). Each hemisphere was then dried at 70°C for 2 days until a constant weight was achieved (dry weight, *D*). An index of edema (*I*) was then calculated as shown in Eq. 1.

$$I = (W/D_L - W/D_R)/(W/D_R) \times 100 \quad (1)$$

This calculation allowed the right hemisphere to serve as a control for the injured left hemisphere in the same mouse.

23. We thank S. Ogawa and Y. Imagawa for the analysis of edema development after cold injury and R. Kado, T. Takahashi, and T. Okada for critical comments on the manuscript. Supported in part by research grants from the Ministry of Education, Science and Culture of Japan; the Ministry of Health and Welfare of Japan; the Science and Technology Agency of Japan; and the Japan Foundation for Neuroscience and Mental Health.

3 January 1997; accepted 2 April 1997

Osmotic Activation of the HOG MAPK Pathway via Ste11p MAPKKK: Scaffold Role of Pbs2p MAPKK

Francesc Posas and Haruo Saito*

Exposure of the yeast *Saccharomyces cerevisiae* to high extracellular osmolarity induces the Sln1p-Ypd1p-Ssk1p two-component osmosensor to activate a mitogen-activated protein (MAP) kinase cascade composed of the Ssk2p and Ssk22p MAP kinase kinase kinases (MAPKKKs), the Pbs2p MAPKK, and the Hog1p MAPK. A second osmosensor, Sho1p, also activated Pbs2p and Hog1p, but did so through the Ste11p MAPKKK. Although Ste11p also participates in the mating pheromone–responsive MAPK cascade, there was no detectable cross talk between these two pathways. The MAPKK Pbs2p bound to the Sho1p osmosensor, the MAPKKK Ste11p, and the MAPK Hog1p. Thus, Pbs2p may serve as a scaffold protein.

MAP kinase cascades are common eukaryotic signaling modules that consist of a MAP kinase (MAPK), a MAPK kinase (MAPKK), and a MAPKK kinase (MAPKKK) (*1*). In *S. cerevisiae*, two independent osmosensors regulate the common HOG (high osmolarity glycerol response) signal transduction pathway, which includes the Pbs2p MAPKK and Hog1p MAPK (*2*–*5*). The Sln1p-Ypd1p-Ssk1p two-component osmosensor uses a multistep phosphorelay mechanism to regulate the redundant MAPKKKs Ssk2p and Ssk22p (*2*, *3*, *6*, *7*). Activated Ssk2p or Ssk22p then phosphorylates and activates the Pbs2p MAPKK. The second osmosensor, Sho1p, contains four transmembrane segments and a COOH-terminal cytoplasmic region with an SRC homology 3 (SH3) domain (*3*). The interaction between an NH_2-terminal proline-rich motif in Pbs2p and the Sho1p SH3

Division of Tumor Immunology, Dana-Farber Cancer Institute, and Department of Biological Chemistry and Molecular Pharmacology, Harvard Medical School, Boston, MA 02115, USA.

*To whom correspondence should be addressed. E-mail: haruo_saito@dfci.harvard.edu